Original article
doi: 10.17223/25421379/36/11

A GEOSPATIAL ANALYSIS OF LAND SURFACE TEMPERATURE AND THE SURFACE URBAN HEAT ISLAND IN TOMSK CITY: A STUDY BASED ON LANDSAT 8 SATELLITE IMAGERY

Clide Marimira

National Research Tomsk State University, Tomsk, Russia, marimira.clyde@gmail.com

Abstract. An urban heat island defines a specific microclimate, where urban areas experience higher temperatures relative to surrounding rural or suburban areas. This phenomenon is linked to reduced wind speeds, alterations in wind direction, reduced urban ventilation and the accumulation of air pollutants within cities, resulting in negative health outcomes to urban residents. In recent years, advancements in thermal remote sensing technologies and the implementation of open data initiatives have prompted numerous investigations into the surface urban heat island.

This study aims to investigate the geospatial distribution of land surface temperature and the surface urban heat island over Tomsk City, during the summer season of 2023. To achieve this, the research utilizes remote sensing imagery obtained from the Thermal Infrared Sensor 1 (TIRS1) and the Operational Land Imager (OLI), both instruments onboard the Landsat 8 Satellite. By applying geospatial analysis and modern satellite remote sensing techniques, including the surface urban heat island index method and zonal statistics, the study aims to; quantify the intensity and spatial extent of surface urban heat island; identify urban hotspots of land surface temperature anomalies and their spatial distribution over land cover and land use classes.

The findings indicate a significant variation in land surface temperature and the surface urban heat island across the research area, with higher land surface temperature and more pronounced surface urban heat island effect predominantly observed in densely built-up areas. Specifically, 83 % of the urban hot spots exhibiting high land surfaces temperature anomalies were observed in densely built-up areas that is urban areas and 16% on bare soil surfaces. Notably, no surface urban heat island was observed in 54 % of the study area, wherein the corresponding major land use and land cover class was vegetation. The mean surface urban heat island intensity, herein the difference between the averages of land surface temperatures between urban and suburban areas ranged between 2°C to 3 °C.

The findings of the study provide valuable insights into the dynamics of land surface temperature and the surface urban heat island effect in Tomsk City. The observed relationships between land surface temperature and surface urban heat island with specific land use and land covers emphasises that vegetation and water surfaces are crucial for reducing urban temperatures and creating favourable microclimate conditions which may consequently increase thermal comfort, and decrease energy consumption.

Keywords: *land surface temperature, surface urban heat island, urban heat island, Landsat 8, urban climate, land use and land cover*

For citation: Marimira C. (2025). A geospatial analysis of land surface temperature and surface urban heat island in Tomsk City: a study based on Landsat 8 satellite imagery. *Geosfernye issledovaniya – Geosphere Research*. 3. pp. 182–196. (In Russian). doi: 10.17223/25421379/36/11

Научная статья
УДК 551.584.2: 551.501.86
doi: 10.17223/25421379/36/11

ГЕОПРОСТРАНСТВЕННЫЙ АНАЛИЗ ТЕМПЕРАТУРЫ ПОВЕРХНОСТИ ЗЕМЛИ И ПОВЕРХНОСТНОГО ГОРОДСКОГО ОСТРОВА ТЕПЛА В ГОРОДЕ ТОМСКЕ: ИССЛЕДОВАНИЕ НА ОСНОВЕ СПУТНИКОВЫХ СНИМКОВ LANDSAT 8

Клайд Маримира

Национальный исследовательский Томский государственный университет, Томск, Россия, marimira.clyde@gmail.com

Аннотация. Городской остров тепла определяет особый микроклимат, при котором в городских районах наблюдается более высокая температура по сравнению с окружающими сельскими или пригородными районами. Данное явление связано с уменьшением скорости ветра, изменением направления ветра, уменьшением вентиляции в городах и накоплением загрязняющих веществ в воздухе, что приводит к негативным последствиям для здоровья городских жителей. В последние годы развитие технологий дистанционного теплового зондирования и реализация инициатив по предоставлению открытых данных привели к многочисленным исследованиям поверхностных городских островов тепла.

Цель данного исследования заключается в том, чтобы исследовать геопространственное распределение температуры поверхности земли и поверхностного городского острова тепла над городом Томском в летний сезон 2023 г. Для достижения этой цели в исследовании используются снимки дистанционного зондирования, полученные с использованием

приборов теплового инфракрасного датчика 1 (TIRS1) и оперативного наземного имиджера (OLI), оба из которых находятся на борту спутника Landsat 8. Применяя Геопространственный анализ и современные спутниковые методы дистанционного зондирования, включая метод индекса поверхностного городского острова тепла и зональную статистику, исследование направлено на количественную оценку интенсивности и пространственной протяженности поверхностного городского острова тепла; выявление городских горячих точек, демонстрирующих высокие аномалии температуры поверхности земли, и их пространственное распределение по классам земного покрова и землепользования.

Полученные данные свидетельствуют о значительном изменении температуры поверхности земли и поверхностного городского острова тепла на всей территории исследования, причем более высокая температура поверхности земли и более выраженный эффект поверхностного городского острова тепла наблюдаются преимущественно в районах плотной застройки. В частности, 83 % городских «горячих точек» аномалий температуры поверхности земли наблюдались над плотно застроенными территориями, т.е. над городскими районами, а 16 % – на голой поверхности почвы. Примечательно, что на 54 % исследуемой территории не наблюдалось поверхностного городского острова тепла, где соответствующим основным классом землепользования и растительного покрова была растительность. Измеренная интенсивность поверхностного городского острова тепла, т.е. средняя температура поверхности городской земли и средняя температура поверхности городской земли в пригороде, составляла от 2 до 3 °C.

Результаты исследования предоставляют ценные сведения о динамике температуры поверхности земли и приземных городских островов тепла в городе Томске. Наблюдаемая взаимосвязь между температурой поверхности земли и поверхностным городским островом тепла с конкретными видами землепользования и растительного покрова говорит о том, что растительность и водные поверхности имеют решающее значение для снижения городских температур и создания благоприятных условий микроклимата, что, в свою очередь, может повысить тепловой комфорт и снизить потребление энергии.

Ключевые слова: *температура поверхности земли, поверхностный городской остров тепла, городской остров тепла, Landsat 8, городской климат*

Для цитирования: Marimira C. A geospatial analysis of land surface temperature and surface urban heat island in Tomsk City: a study based on Landsat 8 satellite imagery // Геосферные исследования. 2025. № 3. С. 182–196. doi: 10.17223/25421379/36/11

Introduction

Urbanization is significantly altering natural landscapes often inadvertently creating an unfavourable microclimate [Crum, Jenerette, 2017; Badugu et al., 2023]. The most notable manifestation of this alteration is the urban heat island (UHI), which has been linked to challenges ranging from public health, energy resources and urban planning [Zhang et al., 2023; Diem et al., 2024].

An urban heat island (UHI) was first observed by a British manufacturing chemist and an amateur meteorologist, Luke Howard, in the early 1833 [Chapman et al., 2017; Zhang et al., 2023]. It defines a specific microclimate, that is characterized by significantly higher temperatures as compared to surrounding rural or suburban areas [Hidalgo-García, Arco-Díaz, 2022; Badugu et al., 2023; Le, Bakaeva, 2023; Diem et al., 2024]. UHI has become a focal point of research and policy discussions due to its many-sided impacts on urban environments and society at large [Liou et al., 2024].

Studies have shown that high temperatures in the urban core centres can intensify the prevalence of heat related deaths and illness especially during heatwaves [Hidalgo-García, Arco-Díaz, 2022; Cleland et al., 2023]. In the United States of America (USA) alone, it is estimated that deaths due to heat exposure ,1500 annually, are more than deaths due dangerous weather phenomena [Hsu et al., 2021].

UHI increases the risk of vulnerable populations, such as the elderly and children, to heat-related health outcomes [Hsu et al., 2021]. These include heat-related illnesses like heat exhaustion, heatstroke and recently more chronic outcomes such as cardiovascular diseases [Hsu et al., 2021; Hidalgo-García, Arco-Díaz, 2022]. Chronic temperature-related diseases, such as comorbid respiratory diseases, cardiovascular diseases, and lung function are most prevalent in high to extreme UHI conditions. An urban heat island is also associated with decreased thermal comfort, and increased energy consumption [Santamouris et al., 2015] for sustaining comfortable temperature particularly in summer or during warmer months [Almeida de et al., 2021; Le, Bakaeva, 2023; Diem et al., 2024]. Therefore, characterising the dynamics of UHI is key for developing effective mitigation strategies and improving urban living conditions.

There are two main types of an urban heat island: the surface urban heat island (SUHI/UHI $_{Surface}$) and the atmospheric urban heat island (UHI) [Badugu et al., 2023; Liou, Tran, Nguyen, 2024]. The atmospheric UHI is often further divided into two forms: the canopy layer urban heat island (CLHI/UHI$_{CL}$) and the boundary layer urban heat island (BLHI/UHI$_{BL}$) [Badugu et al., 2023; Diem et al., 2024; Liou et al., 2024].

The (atmospheric) UHI is measured based on in-situ air temperature (Ta) observations from fixed meteorological stations [Badugu et al., 2023; Liou et al., 2024]. This direct measurement approach provides the best indicator of human experience, but the sparse distribution of monitoring stations can result in insufficient spatial and temporal detail for applied

purposes such as urban planning, public health, energy resources planning and general policy making [Almeida de et al., 2021; Badugu et al., 2023].

In contrast, the Surface UHI (SUHI/UHI $_{surface}$ is based on LST measurements, which are derived from thermal infrared sensors onboard satellites (e.g., Landsat 8/9, Terra, Aqua, and Sentinel 3) aircraft, or drones (Unmanned Aerial Vehicles (UAVs)) [Khorrami, Gunduz, 2020; Almeida de et al., 2021; Zhang et al., 2023]. Consequently, SUHI can provide a spatially continuous representation of LST patterns across urban and rural areas, and across different land covers and land uses, hence can produce sufficient spatial and temporal detail for fundamental and applied purposes [Badugu et al., 2023; Liou et al., 2024].

Advances in thermal remote sensing technology, such as the TIRS1 and TIRS2 instruments on Landsat 8/9, MODIS on Terra and Aqua, and SLSTR on Sentinel 3, combined with open data policies, have facilitated many studies on UHI surface in recent decades [Almeida de et al., 2021; Zhang et al., 2023]. Diem et al. [2024] found 753 publications with the name SUHI/UHI $_{surface}$ in the Web of Science (WoS), Scopus and Google Scholar, more than half of the 753 publications were in the last four years. Additionally, 60.27 % of the 753 studies used Landsat satellite images as primary data sets, an indication that Landsat satellite sensors are well established in SUHI studies.

Previous researches who demonstrated the use of TIRS1 and OLI instruments onboard Landsat 8 satellites in surface urban heat island studies include: Hidalgo-García, Arco-Díaz [2022], who focused on evolution of the surface urban heat island (SUHI) and its driving forces over Granada, Spain. Likewise, in Turkey, Khorrami, Gunduz [2020] studied the seasonal spatial-temporal relations of the Istanbul SUHI with spectral indicators such as, normalized vegetation index (NDVI), tasselled cap wetness (TCW), and surface albedo. In Yerevan, Armenia, researchers investigated the link between land cover and SUHI, methods used to derive land cover and SUHI from Landsat Images included Machine Learning algorithms and the Urban Thermal Field Variance Index (UTFVI), respectively [Tepanosyan et al., 2021].

Equally, in the Russian Federation: Le, Bakaeva [2023] assessed SUHI in Moscow, using Landsat 8 TIRS1 imagery, cloud computing and the UTFVI method to determine the location of urban heat islands, while Korniyenko, Dikareva [2022] identified the UHI surface in the City of Volgograd in summer period using Landsat 8 data and the UHI index method and in the city of Novosibirsk, Gazimov, Kuzhevskaya [2021] estimated the summer surface urban heat island and its drivers using Band 10 of the Landsat 8 TIRS1 and Bands 4 and 5 of OLI instrument. However, the SUHI studies are mainly established in metropolitans and large urbanised cities as compared to smaller cities.

Tomsk city is a relatively small city which is almost 300 km^2. It is the administrative capital of Tomsk region, located in the east of Western Siberia, in the Russian Federation [Official Portal of «The city of Tomsk», 2024].

Seemingly, earlier research implemented in Tomsk City have primarily focused on the (atmospheric) UHI and rather than SUHI [Svarovsky, Starchenko, 2021a, 2021b]. Through the Weather Research and Forecasting model, researchers investigated the UHI in Tomsk City, and the temperature difference between the city and the suburbs was shown to reach 1–3 °C and 1–2 °C respectively.

Previous studies have not (sufficiently) characterised the SUHI/UHI surface, more so in light of the fact that absorption of short-wavelength radiation by the urban surfaces contributes significantly to UHI, accounting for 40–50 % of UHI in summer and 5–15 % in winter [Dudorova, Belan, 2016].

Consequently, this study is realised in an effort to fill this research gap, by analysing the geospatial variation of LST and characterising the UHI $_{surface}$ in Tomsk City, during the summer season of 2023, using imagery from the Thermal Infrared Sensor 1 (TIRS1) (Band 10) and Operational Land Imager (OLI) onboard Landsat 8 Satellite. Additionally, geospatial techniques, that is, the urban heat island index method (UHI index), and zonal statistics are used to; characterise the intensity and spatial extent and of SUHIs; and identify 'urban hot spots' of LST anomalies respectively.

Research Method and Materials

Study Area. The study area is Tomsk City, located at geographical coordinates 56°20′00″ N, 56°42′30″N and 84°19′30″E ,84°45′00″E, [see Fig. 1]. As of the latest data, the population of Tomsk City is approximately 568.5 thousand [Rakhmanova et al., 2021]. The territory is located on the banks of the Tom River, and is the administrative capital of the Tomsk region, located in the east of Western Siberia, in the Russian Federation [Official Portal of «The city of Tomsk», 2024].

According to the Köppen classification system, Tomsk city predominantly exhibits a Dfb climate. This classification is characterized by significant temperature variations, very cold winters and warm summers with consistent precipitation throughout the year. Summers are short [June to August] nonetheless can be fairly warm, with average temperatures in July reaching 19 °C to 22 °C. Infrequently, summer temperatures can exceed 30 °C [Official Portal of «The city of Tomsk», 2024].

Methodology

The method for calculating land surface temperature (LST) were derived from the US Geological Survey website: https://www.usgs.gov/landsat-missions/using-usgs-landsat-level-1-data-product.

The overall methods used in this study are depicted in Fig. 2.

Datasets

The primary data for this research is acquired from the Landsat 8 Satellite instruments; that is the thermal infrared sensor (TIRS) and the Operational Land Imager (OLI) instrument (see Table 1). Data is attained from the United States Geological Survey (USGS) Earth Explorer web portal https://earthexplorer.usgs.gov/.

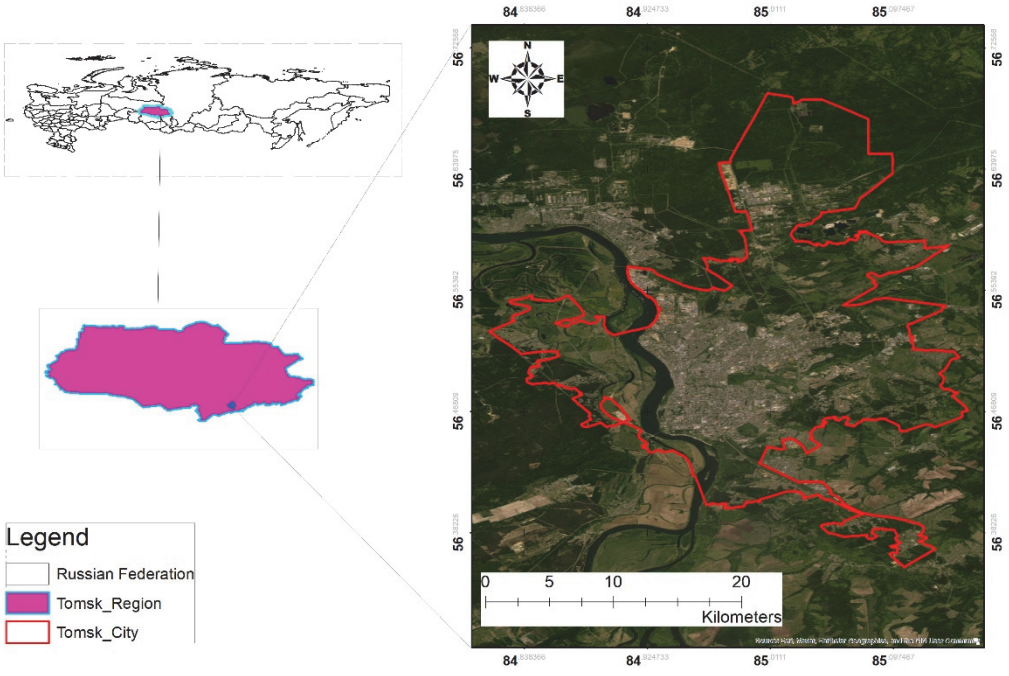

Fig. 1. Study area – Tomsk City

Рис. 1. Район исследования – г. Томск

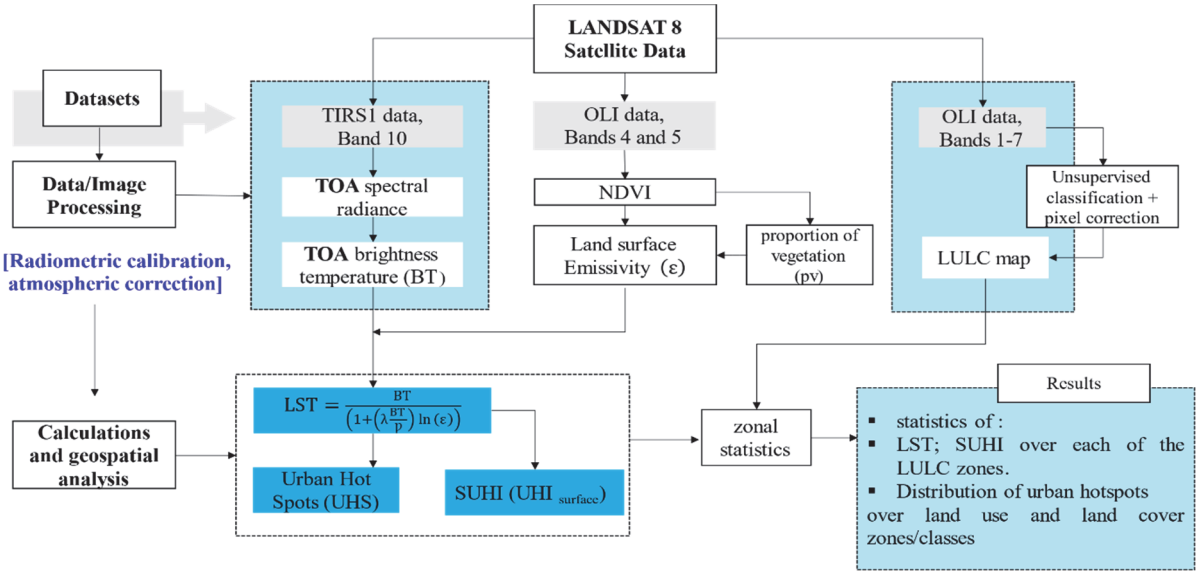

Fig. 2. Research Method

Рис. 2. Метод исследования

Table 1

Description of the Landsat datasets used in this study

Таблица 1

Описание наборов данных Landsat, использованных в данном исследовании

Satellite	Sensor	Cloud cover	Acquisition date and time	Path/row	Spatial resolution
Landsat 8	OLI/TIRS	2.05 %	July 19, 2023; 1030 AM, UTC	147/21	30 m

Calculating the land surface temperature based on Landsat 8 imagery

The first step is to convert $TIRS_1$ Band 10 stored as digital numbers (DNs) to Top of the Atmosphere spectral radiance (ToA spectral radiance) using the formular:

$$L_\lambda = M_L \times Q_{Cal} + A_L \quad (1)$$

where L_λ = ToA spectral radiance [Watts/ (m^2*srad*μm)]; M_L = Band-specific multiplicative rescaling factor from the metadata (MTL.txt); Q_{Cal} = DNs: Band 10 image; A_L= Band-specific additive rescaling factor from the metadata.

The second step is calculating the Top of the Atmosphere brightness temperature (ToA brightness temperature. This involves utilizing the thermal constants provided in the MTL.txt. file.

Equation (2) was used for conversion for the conversion.

$$BT = \left[\frac{K_2}{\ln\left(\frac{K_1}{L_\lambda} + 1\right)}\right] - 273.15, \quad (2)$$

where BT = ToA brightness temperature in Degrees Celsius; L_λ = ToA spectral radiance (Watts/ (m^2 *srad*μm)) calculated in (1); $\mathbf{K_1}$ and $\mathbf{K_2}$ stand for the band-specific thermal conversion constants from the metadata (Table 3).

The third and fourth step is calculating the Normalised Difference Vegetation Index (NDVI) and proportion of vegetation (PV) respectively. To calculate NDVI (3) is used:

$$NDVI = \frac{NIR(Band\ 5) - Red(Band\ 4)}{NIR(Band\ 5) + Red(Band\ 4)} \quad (3)$$

Wherein, Band 5 is the near-infrared band (NIR) from Landsat 8 OLI and Band 4 is the Red band from Landsat 8 OLI. Both NDVI and PV are related to land surface emissivity. In-order to calculate PV, equation (4) was used:

$$PV = \left[\frac{NDVI - NDVI_{min}}{NDVI_{max} - NDVI_{min}}\right]^2, \quad (4)$$

where $NDVI_{min}$ and $NDVI_{max}$ = the minimum and maximum values of the NDVI image, respectively.

Table 2

Metadata; Landsat 8 TIRS (Band 10) Image; $M_L$and $A_L$values

Таблица 2

Метаданные; снимок Landsat 8 TIRS (Band 10); значения M_L and A_L

Variable	Description	Value
M_L	Band-specific multiplicative rescaling factor	3.342×10^{-4}
A_L	Band-specific additive rescaling factor	0.100

Source: Metadata file of Landsat 8 OLI/TIRS [USGS Earth Explorer, 2023].

Table 3

K_1 and K_2 values from the Metadata File of the Landsat 8 Image (TIRS1 Band10)

Table 3

K_1 и K_2 значения из файла метаданных снимка Landsat 8 (TIRS1 Band10)

Variable	Description	Value
K_1	Thermal constant	774.8853
K_2	Thermal constant	1321.0789

Source: Metadata file of Landsat 8 OLI/TIRS [USGS Earth Explorer, 2023].

The fifth step is the calculation of the land surface emissivity (ε) a factor that helps in estimating Land Surface Temperature (LST) by scaling the emitted radiance from the Earth's surface. This scaling factor

allows us to measure how thermal energy is transmitted from the surface into the atmosphere [Young et al., 2017; Zahir, 2020; Hidalgo-García, Arco-Díaz, 2022]. ε is calculated using equation (5):

$$\varepsilon = 0.004 \times Pv + 0.986, \quad (5)$$

where ε = land surface emissivity; P_V = proportion of vegetation calculated in equation (4).

Lastly, the Land surface temperature (LST) can be calculated according to Hidalgo-García, Arco-Díaz [2022] the balanced equation for calculating LST [Young et al., 2017; Almeida de et al., 2021; Gazimov, Kuzhevskaya, 2021] is equation (6).

$$LST = \frac{BT}{\left(1 + \left(\lambda \frac{BT}{p}\right) \ln(\varepsilon)\right)}, \quad (6)$$

where

$$p = \frac{hc}{f}, \quad (7)$$

where BT is ToA brightness temperature calculated in equation [2]; **ε** is corrected land surface emissivity calculated in equation (5); λ = the emitted radiance (λ is 10.895); $p = hc/f = 1.438 \times 10^{-2}$ m K, and h = Planck's constant (6.626×10^{-34} Js); c = speed of light in vacuum (2998×10^{8} m/s); f = Boltzmann's constant (1.38×10^{-23} J/K).

Preparation of a remote sensing-based land use land cover map

Further to that, a remote sensing-based land use and land cover (LULC) map is created according to the method illustrated in Fig. 3.

1. Unsupervised classification based on the ISO Cluster algorithm in QGIS was done, automatically grouping similar pixels into one spectral class.

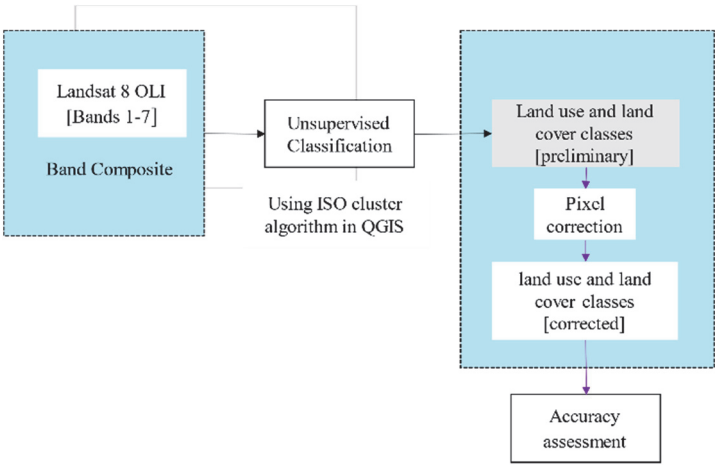

Fig. 3. Land cover land use classification method [Gore et al., 2020; ThanushKodi, Babykalpana, 2010]

Рис. 3. Метод классификации землепользования и земельного покрова

Table 4

SUHI zones

Таблица 4

Зоны SUHI

SUHI zone	1 (no SUHI)	2	3	4	5	6
SUHI index	< 0 °C	0.0–0.5 °C	0.5–1.0 °C	1.0–2.0 °C	2.0–3.0 °C	> 3.0 °C

2. Secondly, pixel-level correction was done, while manually correcting any spectral mixing or or misclassifications. This hybrid method is flexible and can lead to more accurate LULC maps compared to using either approach alone [Gore et al., 2020; ThanushKodi, Babykalpana, 2010; Peacock, 2014].

Characterising the surface urban heat island (SUHI/UHI $_{surface}$)

The surface urban heat island effect (SUHI) over the city of Tomsk was calculated following equation (8) following Siswanto et al. [2023]

$$SUHI = \frac{LST_i - LST_{mean}}{SD} \quad (8)$$

where LSTi = land surface temperature in each pixel of the study area (6); LST_{mean} = is the mean LST of the study area; SD= LST standard deviation of the study area.

In further characterising the surface urban heat islands (SUHI) the following steps are taken:

1. Calculating the predominant land use and land cover types within each SUHI zone.

This information is crucial for identifying which land cover types are prevalent in high SUHI zones versus lower ones [Liu et al., 2023; Moharram, Sundaram, 2023]. Firstly, the SUHI over Tomsk City, calculated in (8) is divided into six classes see Table 4. Area of each class, is calculated in km^2.

Using the zonal statistics overlays majority analysis tool in a QGIS, the SUHI zones in Table 4 [in vector format] are overlayed with a remote sensing based LULC map [in raster format], the results will identify the most frequent pixels of land covers in each of the SUHI classes.

2. Calculating the SUHI intensity based on equation (9) [Siswanto et al., 2023; Liou et al., 2024] and methods as illustrated in Fig. 4.

$$SUHII = LST_{urban} - LST_{rural} \quad (9)$$

In the first method (a), based on SUHI thresholds]; LST_{urban} is referenced from the zonal mean LST in the class where [SUHI>1]; and LST_{rural}= zonal mean LST in the class where [0≤SUHI<1].

The second method (b) is based on LULC map; LST_{urban} and LST_{rural} are referenced from the zonal mean LST in the densely built-up area and the suburban / sparsely built-up area respectively.

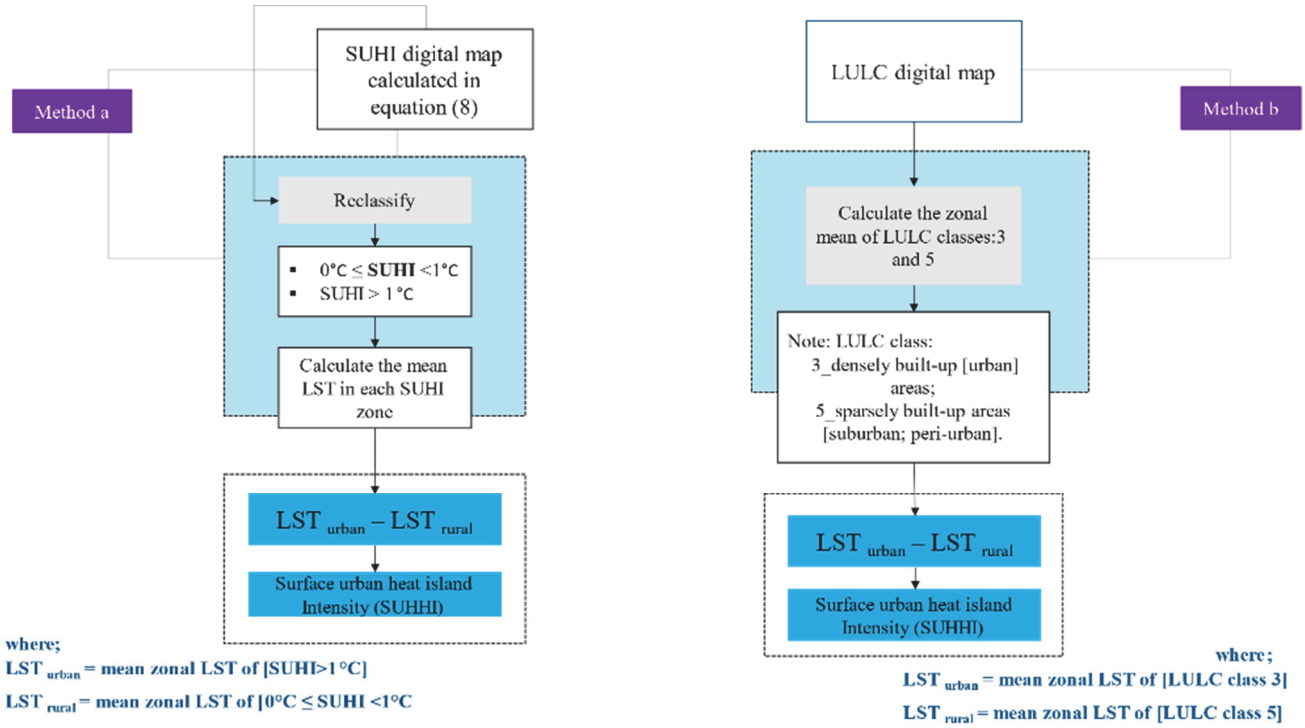

Fig. 4. Methods used to estimate the range of SUHII over the study area

Рис. 4. Методы, используемые для оценки распространения SUHII на исследуемой территории

The Geospatial distribution of urban hotspots (UHS) of LST anomalies

1. Firstly, UHS exhibiting high LST anomalies are calculated from an LST map, based on equation (10) which was derived from [Hidalgo-García, Arco-Díaz, 2022]. The method is illustrated in Fig. 5.

$$LST > \mu + 2 * \sigma, \quad (10)$$

where LST is the land surface temperature in degrees Celsius; μ is the mean (average) LST of the study area, and σ is the standard deviation.

2. Secondly using the zonal statistics overlays tool in a QGIS, the UHS identified in (10) [in vector format] are overlayed with a remote sensing based LULC map [in raster format], the results will show how UHS are spatially distributed over the land use and land covers.

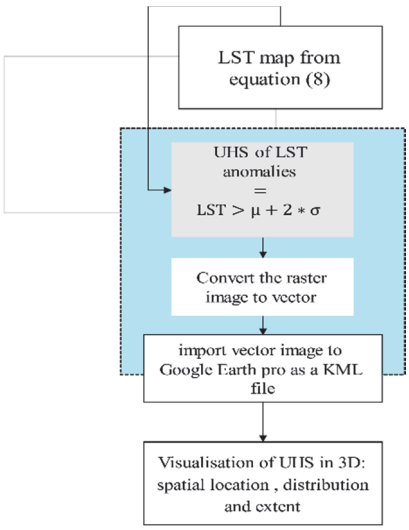

Fig. 5. Method used for estimating the geospatial distribution of UHS [Hidalgo-García, Arco-Díaz, 2022]

Рис. 5. Метод, используемый для оценки геопространственного распределения UHS

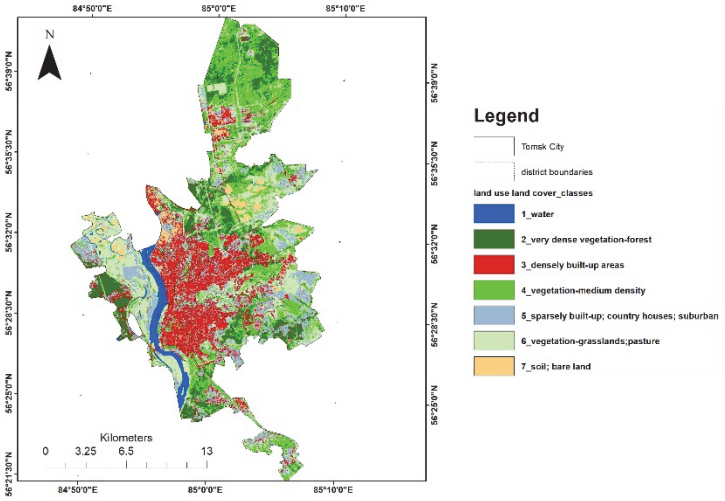

Fig. 6. The land use and land cover map of Tomsk City, created by the author using QGIS software (July 2023)

Рис. 6. Карта землепользования и покрова города Томска, создана автором с помощью программного обеспечения QGIS (июль 2023 г.)

Table 5

Confusion matrix, detailing accuracy assessment of LULC, created by author using QGIS

Таблица 5

Матрица ошибок, подробно описывающая оценку точности LULC, создано автором с использованием QGIS

LULC Class	**1**	**2**	**3**	**4**	**5**	**6**	**7**	Total	**U_Accuracy**	Kappa
1	10	0	0	0	0	0	0	10	1	0
2	0	7	2	0	0	1	0	10	0.7	0
3	0	0	9	0	0	0	1	10	0.9	0
4	0	0	0	9	0	0	2	11	0.82	0
5	0	0	0	0	9	1	0	10	0.9	0
6	0	0	0	0	0	10	1	11	0.91	0
7	0	0	1	0	0	0	9	10	0.9	0
Total	10	7	12	9	9	12	13	72	0	0
P_Accuracy	1	1	0.8	1	0.8	0.8	0.7	0	**0.88**	0
Kappa	0	0	0	0	0	0	0	0	0	**0.85**

Note: **1** – water; **2** – very dense vegetation, forest; **3** – densely built-up areas; **4** – vegetation medium-density; **5** – sparsely built-up, suburban, country houses; **6** – vegetation-grassland, pasture; **7** – soil / bare land; **P_Accuracy** – Producer accuracy. **U_Accuracy** – User accuracy

Примечание: **1** – вода; **2** – очень густая растительность, лес; **3** – густо застроенные районы; **4** – растительность средней плотности; **5** – редкая застройка, пригород, сельские дом; **6** – растительность – луга; пастбища; **7** – почва / голая земля; **P_Accuracy** – точность производителя; **U_Accuracy** – точность пользователя.

Results

Land use and land cover classification

The accuracy assessment of the land use and land cover classification is detailed by the confusion matrix in Table 5.

Variation of land surface temperature (LST) over the study area

LST ranged from a minimum of 14.8 °C to a maximum 39.6 °C. The average LST was 25.60 °C and the standard deviation of 2.78 and significantly varied in the urban space (see Fig. 7 Variation of LST in Tomsk City).

The Table 8 presents data on the LST across different Land Use/Land Cover (LULC) classes in Tomsk City. It includes the minimum, maximum, mean, and standard deviation of LST for seven distinct LULC classes.

The highest mean LST (29.14 °C) and maximum LST (39.64 °C) are observed in the LULC class 3 [densely built-up areas].

While the lowest mean LST (22.34) is observed over LULC class 1 [water].

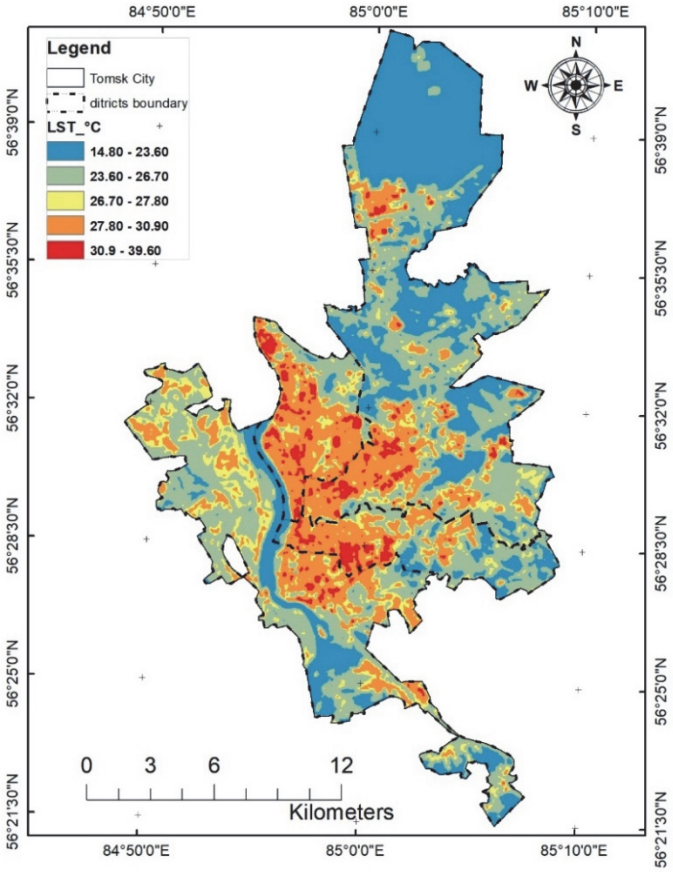

Fig. 7. Variation of LST in Tomsk City

Рис. 7. Изменение LST в городе Томске

Table 6

Geospatial distribution of LST in LULC classes, created by author using QGIS software

Таблица 6

Геопространственное распределение LST в классах LULC, создана автором с помощью программного обеспечения QGIS

LULC Class	1	2	3	4	5	6	7
Min LST °C	21.08	21.4	21.41	21.26	21.9	21.3	21.73
Max LST °C	35.87	34.37	39.64	31.98	34.78	33.03	38.46
Mean LST°C	22.34	23.65	29.14	23.4	27.2	24.75	28.59
Standard deviation	1.34	1.57	1.93	1.46	1.61	1.60	2.07

Note. LULC class **1** – water; **2** – very dense vegetation, forest; **3** – densely built-up areas; **4** – vegetation medium-density; **5** – sparsely built-up, suburban, country houses; **6** – vegetation-grassland, pasture; **7** – soil / bare land.

Примечание. Класс LULC **1** – вода; **2** – очень густая растительность, лес; **3** – густо застроенные территори; **4** – растительность средней плотности; **5** – редко застроенные территории, пригородные, сельские дома; **6** – растительность – луга, пастбища; **7** – почва / голая земля.

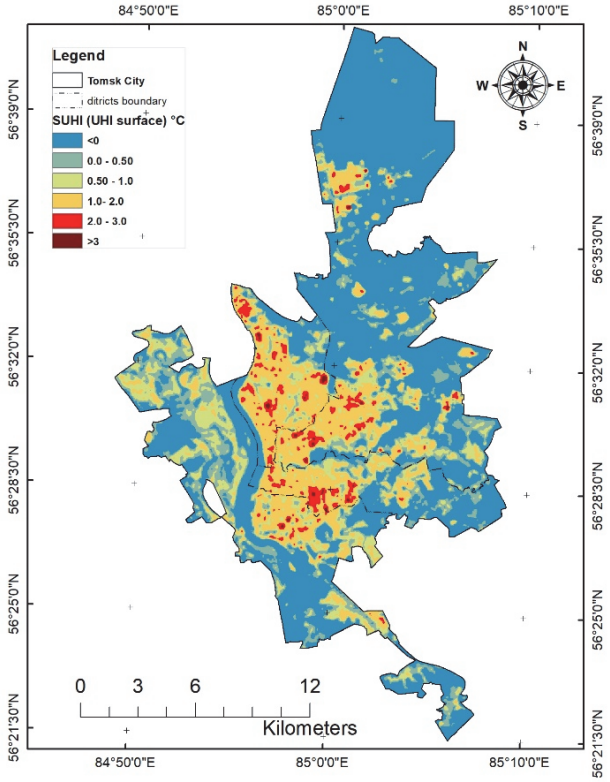

Fig. 8. Spatial variation of SUHI/ $UHI_{surface}$

Рис. 8. Пространственное изменение SUHI/ $UHI_{surface}$

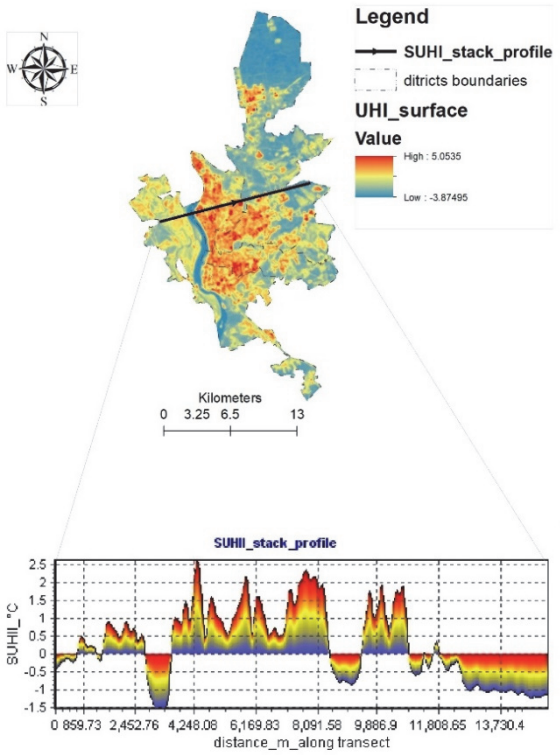

Fig. 9. Surface urban heat island profile along a transect, Tomsk City

Рис. 9. Профиль городского острова тепла на поверхности вдоль трансекты, г. Томск

Table 7

Spatial extent and distribution of SUHI over different land cover types

Таблица 7

Пространственная протяженность и распределение SUHI по различным типам покрова

SUHI index (°C)	<0 [no SUHI]	0.0–0.5	0.5–1.0	1.0–2.0	2.0–3.0	> 3.0 °C
LULC [majority class]	4 **vegetation**	5 **suburban**	5 **suburban**	3 **urban**	3 **urban**	3 **urban**
Extent km^2	160.3953	42.8481	36.0711	48.3687	7.5429	0.4995
% Of study area	54.237	14.489	12.19749	16.35594	2.550	0.168

Spatial distribution of the surface urban heat island (SUHI)

Table 7, provides quantitative data on the extent and distribution of SUHI across various LULC classes. This table highlights quantitatively, how different land cover types contribute to the intensity of the SUHI effect.

While Fig. 9, below complements Table 7 by providing a spatial perspective on how SUHI manifests across the urban landscape not only by land use type but also across geographic locations within Tomsk.

The transect reveals peaks in SUHI corresponding to land covers identified in Table 7 as having high SUHI values, such as urban areas or densely built-up areas.

Fig. 9 also shows a significant temperature decrease at specifics points along the transect, this can be correlated with low values from Table 7, that correspond to specific LULC class (e.g., water).

The SUHI profile along an east-to-west transect typically starts with low values in rural areas at both ends, peaks in the densely built-up urban core, and gradually declines back toward rural zones.

The Fig. 10 presents data on the Mean Surface Urban Heat Island (SUHI) effect and its standard deviation across different Land Use/Land Cover (LULC) classes in Tomsk City. Densely Built Areas (Class 3) exhibit the highest mean SUHI value of 1.27°C, Conversely, Water (Class 1) and Dense Vegetation (Class 2) show negative mean SUHI values of –1.12°C and –0.71°C, indicating a cooling effect. The standard deviation values reflect the variability of the SUHI effect within each LULC class.

Surface urban heat island intensity

Based on methods a and b as described Fig. 4; the surface urban heat island intensity (SUHI intensity) calculated as mean LST differences between urban and suburban areas ranged between 2.0 °C to 3.0°C (see Table 8).

Urban hot spots of LST anomalies (UHS)

Fig. 12, shows that, urban hot spots exhibiting LST anomalies (UHS) were not observed over LULC class 1 (water), LULC class 2 (very dense vegetation/forest) and LULC class 6 (grassland; pastures; agricultural land).

Complimentary data, from Fig. 13 below indicates that the largest area of UHS is found in Class 3 (densely built-up class), covering approximately 7.24 km², which constitutes 83.12 % of the total UHS identified in this study. The identity of the urban hot spots (UHS) of high LST anomalies include, shopping malls and industrial sites, the Tomsk Cable Plant and Tomsk Concrete mixing Plant, wherein the highest LST of 39.6 °C (see Fig. 14).

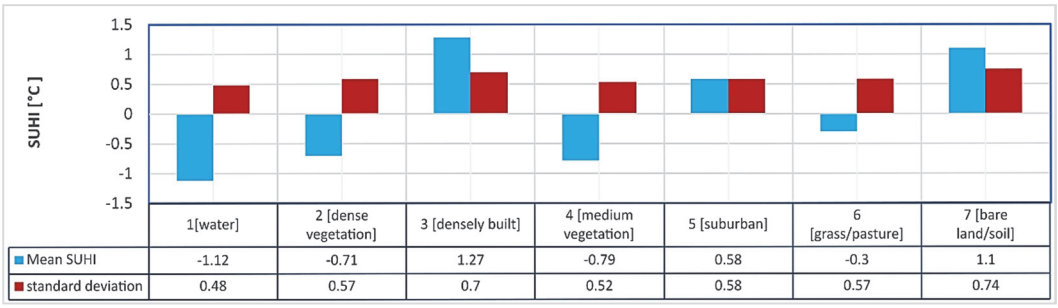

	1[water]	2 [dense vegetation]	3 [densely built]	4 [medium vegetation]	5 [suburban]	6 [grass/pasture]	7 [bare land/soil]
Mean SUHI	-1.12	-0.71	1.27	-0.79	0.58	-0.3	1.1
standard deviation	0.48	0.57	0.7	0.52	0.58	0.57	0.74

Fig. 10. Distribution of SUHI over land use covers

Рис. 10. Распределение SUHI по землепользованию

Table 8

SUHI intensity

Таблица 8

Интенсивность SUHI

SUHI threshold [method a] from Table 7	Zonal average LST °C	Land use land cover map [method b]	Zonal average LST °C
SUHI > 1 [urban]	29.90	Densely built-up areas	29.14
0 ≤ SUHI < 1 [suburban]	26.91	Sparsely built-up / suburban	27.20
mean LST difference (SUHII)	**3.0**	Mean LST difference (SUHII)	**2.0**

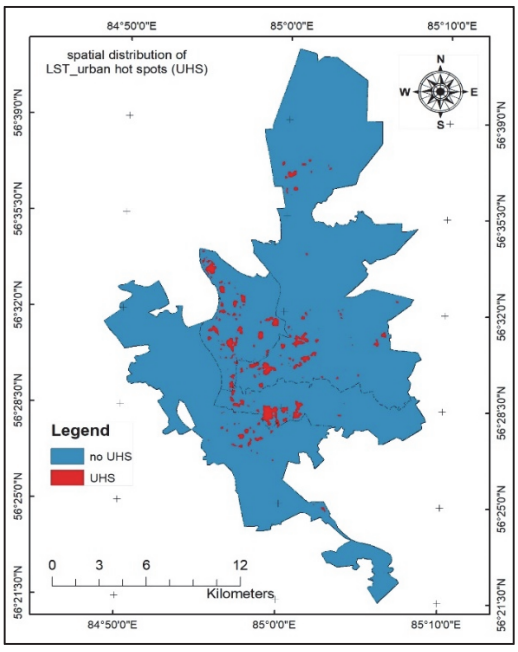

Fig. 11. Geospatial distribution of UHS

Рис. 11. Геопространственное распределение UHS

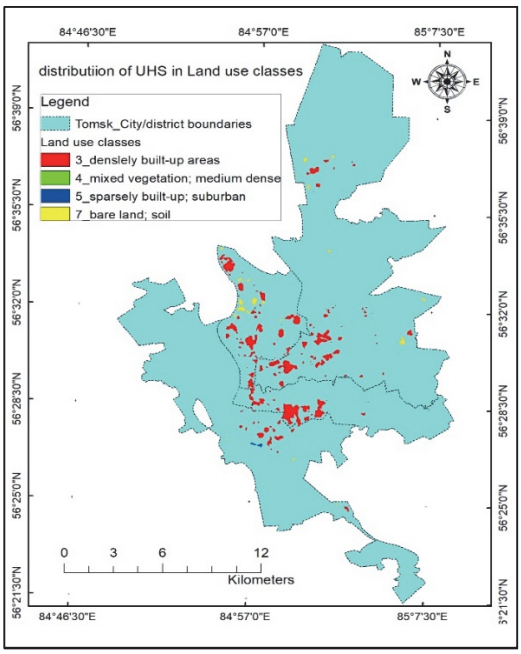

Fig. 12. Spatial distribution of UHS over LULC classes

Рис. 12. Пространственное распределение UHS по классам LULC

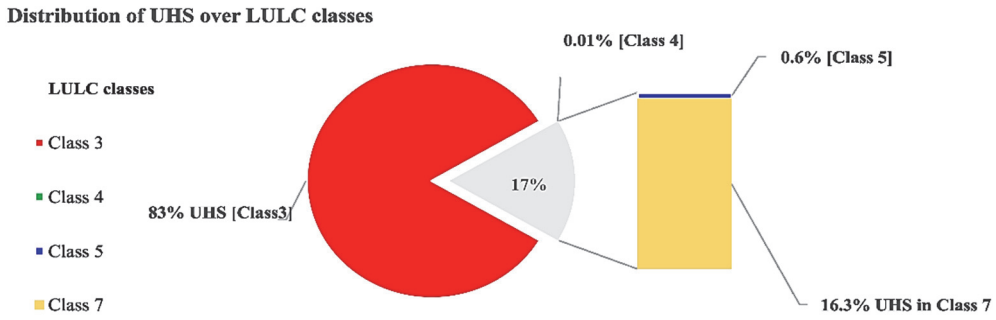

Fig. 13. Distribution of UHS over land use and land cover classes

LULC class **1** – water; **2** – very dense vegetation, forest; **3** – densely built-up areas; **4** – vegetation medium-density; **5** – sparsely built-up, suburban, country houses; **6** – vegetation-grassland, pasture; **7** – soil / bare land

Рис. 13. Распределение UHS по классам землепользования и покрова

Классы LULC: **1** – вода; **2** – очень густая растительность, лес. **3** – густо застроенные районы; **4** – растительность средней плотности; **5** – редкая застройка, пригород, сельские дом; **6** – растительность – луга; пастбища; **7** – почва / голая земля

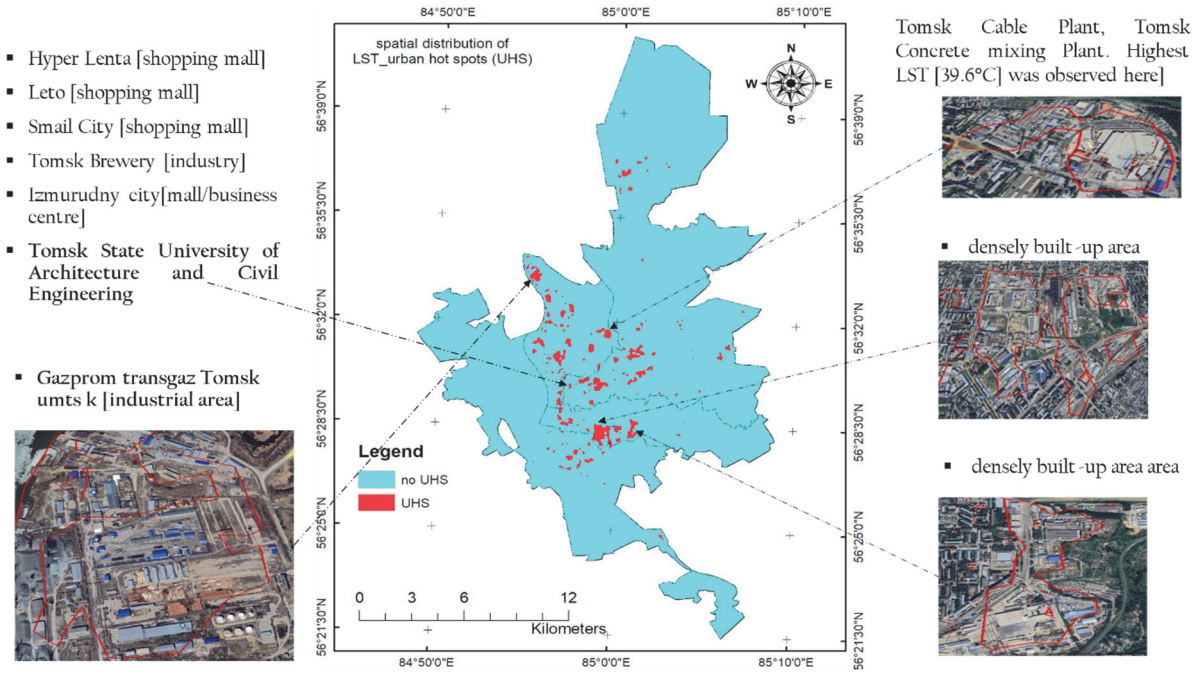

Fig. 14. Urban Hot Spots of land surface temperature anomalies, created by the author using QGIS software

Рис. 14. Городские горячие точки аномалий температуры поверхности земли, создана автором с помощью программного обеспечения QGIS

Discussion

Land surface temperature (LST) distribution

The current study reveals a significant spatial heterogeneity in LST over the study area, wherein higher land surface temperatures were predominantly observed in densely built-up areas and lower land surface temperatures in vegetated and water surfaces [see Table 6 and Fig. 7]. This trend is consistent with previous research [Crum, Jenerette, 2017; Almeida de et al., 2021; Tepanosyan et al., 2021; Karyati et al., 2022; Korniyenko, Dikareva, 2022; Badugu et al., 2023; García et al., 2023].

The high LSTs in densely built-up areas can be attributed to their thermal properties. Urban surfaces are characterized by a higher proportion of dark and impervious material such as asphalt, concrete, and buildings, which absorb and retain more solar radiation leading to increased surface temperatures [Dudorova, Belan, 2016; Li et al., 2023; Diem et al., 2024; Thammaboribal, 2024]. Conversely, vegetated and water surfaces have a higher capacity to reflect and dissipate

heat efficiently through processes such as evapotranspiration, resulting in lower LST values [Zahir, 2020; Kuzhevskaya, 2021; Costanzini et al., 2022; Gazimov, Hidalgo-García, Arco-Díaz, 2022; Korniyenko, Dikareva, 2022; Le, Bakaeva, 2023; Zhang et al., 2023; Liou et al., 2024].

Significance of findings: high LSTs in densely built-up areas can have public health implications [Cleland et al., 2023; Le, Bakaeva, 2023]. For instance, intensifying the prevalence of heat related deaths and illness (heatstroke, dehydration and cardiovascular diseases) [Hsu et al., 2021]. The lower LST observations in vegetated areas suggest the crucial role that green spaces or vegetation plays in moderating urban temperatures; this suggests incorporating vegetation into urban design can help mitigate the warming effects of impervious surfaces and consequently reduce energy consumption in the urban centres of Tomsk during summer months [Zhou et al., 2019; Almeida de, Teodoro, Gonçalves, 2021].

Surface urban heat island effect and its distribution (SUHI)

The study demonstrates the presence of a surface urban heat island effect (SUHI) [see Fig. 8, Fig. 9 and Table 7] in Tomsk city. The SUHI effect covers a spatial extent of 47.8% of the city, with built-up areas comprising the majority of the pixels [see Table 7]. In contrast, 54.2 % of the city shows no SUHI effect and is dominated by vegetation as the majority land cover type [see Table 7]. This implies that vegetation cover reduces SUHI effect. Densely built-up areas and bare soil or bare land surfaces had the highest mean SUHI effect [see Fig. 10], whereas land covers of vegetation and water had a negative SUHI effect, highlighting the decisive role that vegetation and water surfaces play in moderating urban temperatures.

These geospatial distribution of SUHI observed in this study are consistent with previous studies conducted in various urban settings, such as Moscow, Russia [Le, Bakaeva, 2023], Yerevan, Armenia [Tepanosyan et al., 2021], and Novosibirsk, Russia [Gazimov, Kuzhevskaya, 2021].

The SUHI intensity observed in this study [see Table 8] aligns with observations made by Svarovsky, Starchenko, [2021b] , who found a 1–3 °C difference between the urban and suburban areas of Tomsk city in summer season.

The implications of these observations are significant to public health, land use planning and energy consumption. Higher temperatures due to the SUHI effect in the urban setup can lead to decreased thermal comfort, increased energy demand for cooling, especially during the summer months, impacting on both economic costs and environmental sustainability [Badugu et al., 2023; Cleland et al., 2023; Diem et al., 2024].

Identification of UHS distribution in relation to LULC

The study's findings, as illustrated in Fig. 11 and Fig. 12, indicate Urban Hot Spots (UHS) of LST anomalies in Tomsk city. UHS were predominantly observed over specific land use and land covers (LULC). For instance, 83 % of UHS were observed in densely built-up areas/ urbanized areas and 16.3 % in bare soil/ bare land (see Fig. 12, Fig. 13). Furthermore, an absence of UHS over land use classes associated with water bodies and vegetation was noted. This observation aligns with previous research conducted by Hidalgo-García, Arco-Díaz [2022].

Significance and implications of the observations: the comparatively high percentage of UHS found in bare land areas (16.29 %) suggests that even non-urbanized areas can contribute to local heat retention, indicating a need for careful management of these spaces to prevent exacerbating heat effects.

Conclusions

Application of Landsat 8 and Geospatial Techniques for Urban Heat Analysis: the study demonstrates the application of Landsat 8 satellite imagery and geospatial techniques for analysing the geospatial variation of LST and characterising the SUHI effect in Tomsk City, during the summer season of 2023. The research highlights critical insights into how different types of land use and land cover influence urban heat dynamics, which has significant implications for public health and urban planning.

Key findings on LST and SUHI distribution include the fact, that higher LSTs and SUHI effect are predominantly observed in densely built-up or urbanized areas. In contrast, no SUHI effect was observed in 54 % of Tomsk's area, where vegetation dominated the land cover [see Table 6, Fig. 7].

This finding underscores the critical role that green spaces (such as parks, forests, and vegetated areas) and water bodies play in regulating temperature distribution. These natural features help mitigate urban heat by reducing surface temperatures. Hence, by prioritizing green spaces and sustainable land use practices, Tomsk can enhance its resilience against rising temperatures and improve overall quality of life for its residents.

Surface urban heat island (SUHI) Intensity

The observed Surface Urban Heat Island (SUHI) intensity in Tomsk city during the summer reveals a temperature difference of 2–3 °C between urban and

suburban areas [see Table 8]. This indicates a substantial SUHI effect which can have adverse impacts on human health, energy consumption, and the environment. These results can inform on urban planning and decision-making processes for mitigation.

Geospatial distribution of urban hot spots (UHS) displaying high LST anomalies

The study identifies specific areas within Tomsk city that are more vulnerable to heat stress, which can have adverse impacts on human health, energy consumption, and the environment.

The correlation between UHS locations and specific LULC classes underscores a critical urban environmental issue: densely built-up areas and bare soil areas often lack green spaces or water bodies that could otherwise mitigate heat through processes such as evapotranspiration.

The identification of UHS within Tomsk city, particularly their association with specific LULC types, is crucial for developing effective mitigation strategies aimed at reducing urban heat effects.

Overall, the predominant presence of UHS in densely built-up areas and their absence in vegetation and water surfaces can be applied in urban planning interventions, through incorporating green spaces and water bodies to alleviate heat stress in localities where UHS were most observed.

References

Almeida C.R. de, Teodoro A.C., Gonçalves A. Study of the urban heat island (Uhi) using remote sensing data/techniques: A systematic review // Environments - MDPI. 2021. V. 8, No. 10. doi: 10.3390/environments8100105

Badugu A. et al. Spatial and temporal analysis of urban heat island effect over Tiruchirappalli city using geospatial techniques // Geod Geodyn. 2023. V. 14. No. 3. pp. 275–291. doi: 10.1016/j.geog.2022.10.004

Chapman S. et al. The impact of urbanization and climate change on urban temperatures: a systematic review // Landsc Ecol. 2017. V. 32, No. 10. C. doi: 1921–1935. doi: 10.1007/s10980-017-0561-4

Cleland S.E. et al. Urban heat island impacts on heat-related cardiovascular morbidity: A time series analysis of older adults in US metropolitan areas // Environ Int. 2023. V. 178. pp. 108005. doi: 10.1016/j.envint.2023.108005

Costanzini S. et al. Identification of SUHI in Urban Areas by Remote Sensing Data and Mitigation Hypothesis through Solar Reflective Materials // Atmosphere (Basel). 2022. V. 13. 1. doi: 10.1175/JAMC-D-17-

Crum S.M., Jenerette G.D. Microclimate Variation among Urban Land Covers: The Importance of Vertical and Horizontal Structure in Air and Land Surface Temperature Relationships // Journal of Applied Meteorology and Climatology. 2017. V. 56, No. 9. pp. 2531–2543. doi: 10.1175/JAMC-D-17-

Diem P.K. et al. Remote sensing for urban heat island research: Progress, current issues, and perspectives // Remote Sens Appl. 2024. V. 33. doi: 10.1016/j.rsase.2023.101081

Dudorova N.V., Belan B.D. *Ocenka faktorov, opredeljajushhih formirovanie gorodskogo ostrova tepla v Tomske* [Estimation of factors determining formation of the urban heat island in Tomsk] // *Optika atmosfery i okeana* [Atmospheric and ocean optics]. 2016. V. 29, No. 5. pp. 426–436. In Russian. doi: 10.15372/AOO20160510

García D.H., Riza M., Díaz J. A. Land Surface Temperature Relationship with the Land Use/Land Cover Indices Leading to Thermal Field Variation in the Turkish Republic of Northern Cyprus // Earth Systems and Environment. 2023. V. 7, No. 2. pp. 561–580. doi: 10.1007/s41748-023-00341-5

Gazimov T.F., Kuzhevskaya I. V. *Ocenka letnego poverhnostnogo gorodskogo ostrova tepla goroda Novosibirsk po dannym Landsat 8* [Assessment of the summer surface urban heat island of the city of Novosibirsk according to Landsat 8 data] // *Geograficheskiy vestnik* [Geographical Bulletin]. 2021. V. 4, No. 59. pp. 84–98. In Russian. doi: 10.17072/2079-7877-2021-4-84-98

Gore R.W. et al. *Analiz zemlepol'zovaniya s ispol'zovaniem nekontroliruemoy klassifikacii* [LULC-Analysis of land-use with the help of unsupervised classification] // Izvestiya SFedU. Engineering sciences. 2020. No. 3. pp. 184–192. In Russian. doi: 10.18522/2311-3103-2020-3-184-192

Hidalgo-García D., Arco-Díaz J. Modeling the Surface Urban Heat Island (SUHI) to study of its relationship with variations in the thermal field and with the indices of land use in the metropolitan area of Granada (Spain) // Sustain Cities Soc. 2022. V. 87. doi: 10.1016/j.scs.2022.104166

Hsu A. et al. Disproportionate exposure to urban heat island intensity across major US cities // Nature Communications 2021 12:1. 2021. V. 12, No. 1. pp. 1–11. doi: 10.1038/s41467-021-22799-5

Karyati N.E. et al. Application of Landsat-8 OLI/TIRS to assess the Urban Heat Island (UHI) // IOP Conference Series: Earth and Environmental Science.: Institute of Physics, 2022. doi: 10.1088/1755-1315/1109/1/012069

Khorrami B., Gunduz O. Spatio-temporal interactions of surface urban heat island and its spectral indicators: a case study from Istanbul metropolitan area, Turkey // Environ Monit Assess. 2020. V. 192, No. 6. doi: 10.1007/S10661-020-08322-1

Korniyenko S., Dikareva E. Optical Remote Sensing for Urban Heat Islands Identification; 2022; Construction of Unique Buildings and Structures // Construction of Unique Buildings and Structures. 2022. V. 104. No. 10404. doi: 10.4123/CUBS.104.4

Le M.T., Bakaeva N.A. Technique for Generating Preliminary Satellite Data to Evaluate SUHI Using Cloud Computing: A Case Study in Moscow, Russia // Remote Sens (Basel). 2023. V. 15, No. 13. doi: 10.3390/rs15133294

Li X., Chakraborty T.C., Wang G. Comparing land surface temperature and mean radiant temperature for urban heat mapping in Philadelphia // Urban Clim. 2023. V. 51. doi: 10.1016/j.uclim.2023.101615

Liou Y.A., Tran D.P., Nguyen K.A. Spatio-temporal patterns and driving forces of surface urban heat island in Taiwan // Urban Clim. 2024. V. 53. pp. 101806. doi: 10.1109/TGRS.2023.3285912

Liu S. et al. Land Use and Land Cover Mapping in China Using Multimodal Fine-Grained Dual Network // IEEE Transactions on Geoscience and Remote Sensing. 2023. V. 61. pp. 1–19. doi: 10.1109/TGRS.2023.3285912

Moharram M., Sundaram D. Land Use and Land Cover Classification with Hyperspectral Data: A comprehensive review of methods, challenges and future directions // Neurocomputing. 2023. V. 536.

Official Portal of «The city of Tomsk»http://en.admin.tomsk.ru/ [Electronic resource]. URL: http://en.admin.tomsk.ru/ (Date of accessed: 01.06.2024).

Peacock R. Accuracy assessment of supervised and unsupervised classification using Landsat imagery of little rock, Arkansas a thesis presented to the department of humanities and social sciences in candidacy for the degree of Master of Science, 2014.

Rakhmanova L. et al. Perspectives of climate change: A comparison of scientific understanding and local interpretations by different Western Siberian communities // Ambio. 2021. V. 50. No. 11. pp. 2072–2089. doi: 10.1007/s13280

Santamouris M. et al. On the impact of urban heat island and global warming on the power demand and electricity consumption of buildings – A review // Energy Build. 2015. V. 98. pp. 119–124.

Siswanto S. et al. Spatio-temporal characteristics of urban heat Island of Jakarta metropolitan // Remote Sens Appl. 2023. V. 32. doi: 10.1016/j.rsase.2023.101062

Svarovsky A.I., Starchenko A.V. Application of a Weather Research and Forecasting model to study the urban heat island in Tomsk // Journal of Physics: Conference Series.: IOP Publishing Ltd, 2021b.

Svarovsky A.I., Starchenko A.V. *Primenenie modeli weather research and forecasting dlya issledovaniya yavleniya «ostrov tepla» dlya usloviy goroda Tomsk* [Application of the Weather Research and Forecasting model to study the "heat island" phenomenon for the conditions of the city of Tomsk] // *xviii mezhdunarodnaja konferenciya studentov, aspirantov i molodyh uchenyh «perspektivy razvitiya fundamental''nyh nauk»* [the XVIII International Conference of Students, Postgraduate Students and Young Scientists]: *Nacional'niy issledovatel'skiy Tomskiy politehnicheskiy universitet* [National Research Tomsk Polytechnic University]. 2021a. V. 3. pp. 76–78. In Russian

Tepanosyan G. et al. Studying spatial-temporal changes and relationship of land cover and surface Urban Heat Island derived through remote sensing in Yerevan, Armenia // Build Environ. 2021.

Thammaboribal P. Investigating Land Surface Temperature Variation and Land Use Land Cover Changes in Pathumthani, Thailand (1997–2023) using Landsat Satellite Imagery: A Comprehensive Analysis of LST and Urban Hot Spots (UHS) // International Journal of Geoinformatics. 2024. V. 20. No. 2. pp. 27–41.

ThanushKodi K., Babykalpana Y. Supervised/ Unsupervised Classification of LULC using remotely Sensed Data for Coimbatore city, India, 2010. 975–8887 p.

U.S. Geological Survey. Landsat 8 metadata [Электронный ресурс]. 2023. URL: https://earthexplorer.usgs.gov (Date of accessed: 14.03.2024).

Young N. E. et al. A survival guide to Landsat pre-processing // Ecology. 2017. V. 98. No. 4. pp. 920–932.

Zahir I. L. M. Application of Geo-informatics Technology to Access the Surface Temperature Using LANDSAT 8 OLI/TIRS Satellite Data: A Case Study in Ampara District in Sri Lanka. 2020.

Zhang J., Tu L., Shi B. Spatiotemporal Patterns of the Application of Surface Urban Heat Island Intensity Calculation Methods // Atmosphere (Basel). 2023. V. 14. No. 10.

Information about the author:
Marimira C., Master's student, Department of Meteorology and Climatology, Faculty of Geology and Geography, National Research Tomsk State University, Tomsk, Russia.
E-mail: marimira.clyde@gmail.com

The author declares no conflicts of interests.

Информация об автора:
Маримира К., магистрант, кафедра метеорологии и климатологии, геолого-географический факультет, Национальный исследовательский Томский государственный университет, Томск, Россия.
E-mail: marimira.clyde@gmail.com

Автор заявляет об отсутствии конфликта интересов.

Статья поступила в редакцию 23.10.2024; одобрена после рецензирования 17.01.2025; принята к публикации 29.08.2025

The article was submitted 23.10.2024; approved after reviewing 17.01.2025; accepted for publication 29.08.2025